



Decoupling of the Arctic Oscillation and North Atlantic Oscillation in a warmer climate

Mostafa E. Hamouda ^{1,2,3}✉, Claudia Pasquero ^{1,4} and Eli Tziperman ⁵

The North Atlantic Oscillation and the Arctic Oscillation are modes of climate variability affecting temperature and precipitation in the mid-latitudes. Here we use reanalysis data and climate model simulations of historical and warm climates to show that the relationship between the two oscillations changes with climate warming. The two modes are currently highly correlated, as both are strongly influenced by the downward propagation of stratospheric polar vortex anomalies into the troposphere. When considering a very warm climate scenario, the hemispherically defined Arctic Oscillation pattern shifts to reflect variability of the North Pacific storm track, while the regionally defined North Atlantic Oscillation pattern remains stable. The stratosphere remains an important precursor for North Atlantic Oscillation, and surface Eurasian and Aleutian pressure anomalies precede stratospheric anomalies. Idealized general circulation model simulations suggest that these modifications are linked to the stronger warming of the Pacific compared with the slower warming of the Atlantic Ocean.

The positions of the storm track and the seasonal precipitation over Europe and Eastern North America are known to be linked to the phase of the North Atlantic Oscillation (NAO) which is the most prominent pattern of atmospheric variability over middle and high latitudes in the Northern Hemisphere. The NAO is described as an alternation between two pressure systems, the Azores High and the Icelandic Low, which in turn influences weather conditions over large areas^{1,2}. The Arctic Oscillation (AO), also known as the Northern Annular Mode, NAM) has been introduced^{3–5} as a hemispheric climate variability pattern characterized by a primary centre of action over the Arctic and two opposite centres of action in mid-latitudes, one over the North Pacific and the other over the North Atlantic. A negative AO is usually associated with pronounced meridional wind patterns and has been linked with the occurrence of surface extremes in the mid-latitudes⁶. Despite the annular (zonally symmetric) structure that characterizes the AO, sea-level pressure (SLP) anomalies in the North Atlantic and North Pacific centres of action are not correlated⁷, suggesting that each one of them can exist independently of the other.

The present-day monthly temporal correlation between AO and NAO is very high, with correlation coefficients up to 0.95 (refs. ^{8,9}). For this reason, the NAO is often referred to as the local manifestation of the AO and the two terms have been used interchangeably (for example, refs. ^{6,10–12}). Their variability has been shown to be affected by stratospheric anomalies: in winter, the correlation between the 90-d low pass filtered anomalies of 10 hPa and 1,000 hPa geopotential height (GPH) exceeds 0.65, when surface anomaly time series are lagged by about 3 weeks, meaning that stratospheric anomalies are good precursors to surface NAO/AO conditions^{11,13}. On the other hand, the stratospheric polar vortex is known to be influenced by various tropospheric phenomena, such as tropical and extratropical variability, including El Niño/Southern Oscillation (ENSO)¹⁴, Quasi-Biennial Oscillation (QBO)¹⁵, the Madden–Julian tropical atmospheric oscillation (MJO)^{16–18} and sea-ice or snow cover changes in the Arctic region^{19–25}. Enhanced

air–sea fluxes and/or deep convection generate a delayed warming response in the polar stratosphere, which eventually often triggers a negative NAO/AO phase^{16,21,23,26}.

In this study, we analyse the dependence of AO and NAO on climate mean state, showing that their correlation breaks down in a warmer climate and suggesting a sufficient condition for the change. Then, we discuss the implications of these modifications on the stratosphere–troposphere coupling. For this purpose, we analyse the results obtained from the Coupled Model Intercomparison Project Phase 5 (CMIP5) for the historical climate and for the Representative Concentration Pathway8.5 (RCP8.5) scenario, and from simulations of an intermediate complexity model, and compare them to reanalysis data. We compare the present-day climate with the most extreme climatic scenario of RCP8.5 during the twenty-third century. We choose this time frame to shed light on the theoretical behaviour of these coupled modes of variability and demonstrate that they can behave very differently under large climate forcing.

Decoupling of the AO and NAO

Wintertime SLP climatology is characterized by the Aleutian low pressure in the North Pacific, and the (deeper) Icelandic low-pressure centre in the North Atlantic, with a high-pressure centre over the polar cap, as in the contours of Fig. 1a,b. The variability of the Atlantic and the Pacific pressure systems are of similar magnitudes in the current climate (shading in Fig. 1a,b).

The Icelandic and the Aleutian low-pressure systems represent the main centres of action of the AO mode of variability³ as the leading mode of the Empirical Orthogonal Function (EOF) analysis of SLP of the hemisphere north of 20°N. Similarly, the NAO is defined²⁷ as the first EOF of SLP in the domain (20°N–80°N, 90°W–40°E). The EOF analysis is performed using monthly mean SLP for boreal winter (December, January and February (DJF)). It is worth stressing that EOFs are statistical patterns defined to most efficiently characterize the covariability of the system but they do

¹Department of Earth and Environmental Sciences, Università di Milano Bicocca, Milan, Italy. ²Astronomy and Meteorology Department, Faculty of Science, Cairo University, Cairo, Egypt. ³Osservatorio Geofisico Sperimentale, Trieste, Italy. ⁴Istituto di Scienze dell'Atmosfera e del Clima, Consiglio Nazionale delle Ricerche, Turin, Italy. ⁵Department of Earth and Planetary Sciences and School of Engineering and Applied Sciences, Harvard University, Cambridge, MA, USA. ✉e-mail: m.hamouda@campus.unimib.it

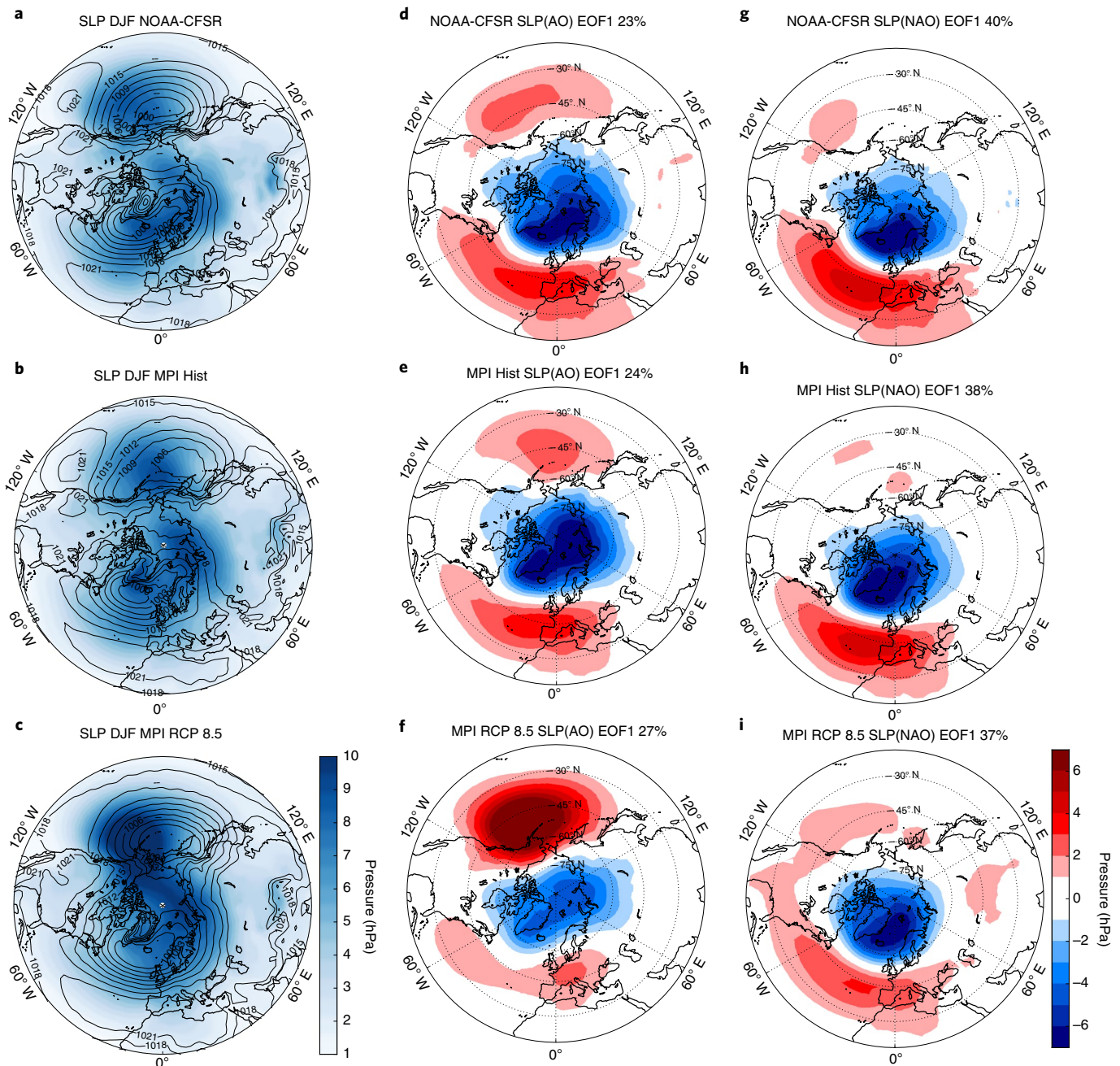


Fig. 1 | SLP climatology and modes of variability. **a–c**, Wintertime DJF monthly mean SLP (contours in hPa), and standard deviation (s.d.; shading in hPa) for NOAA-CFSR reanalysis (**a**) and MPI-ESM-LR historical (Hist) (**b**) and RCP 8.5 (**c**). **d–f**, The leading EOF mode (AO) for DJF SLP for NOAA-CFSR reanalysis (**d**) and MPI-ESM-LR Hist (**e**) and RCP 8.5 (**f**). Panels **g–i** are similar to **d–f** except that global SLP is regressed onto the NAO index. The explained variance by the EOF is indicated on top of each panel. Note that the explained variance of **g–i** refers only to the variability in the North Atlantic sector. Shading unit: hPa, corresponding to 1 s.d. of the PC.

not necessarily represent a physical mechanism nor relate to real causal connections among different regions. Notice that with these definitions of AO and NAO, the variability patterns can be different in a different climate and no link with the patterns identified in the current climate is prescribed.

The observed AO and NAO patterns in the state-of-art reanalysis (NOAA-CFSR)²⁸ are shown in Fig. 1d,g, on the basis of the period from 1979 to 2018. The historical period is simulated by CMIP5 models from 1901 to 2000. Visual inspection of the variability patterns computed from the simulation outputs indicates a good

agreement between CMIP5 models and reanalysis (Fig. 1e,h and Extended Data Fig. 1), apart from the model GISS-E2-R, in which the AO pattern has a rather weak centre of action over the Atlantic.

A quantification of the performance of CMIP5 models in representing variability patterns in the historical simulations is obtained by computing the spatial correlation between the EOFs derived from the models and from the NOAA-CFSR reanalysis. Results indicate that in all cases, correlation coefficients are >0.87 (Fig. 2a).

The patterns of variability in CMIP5 models were also computed in the RCP 8.5 scenario and results are shown for the period from

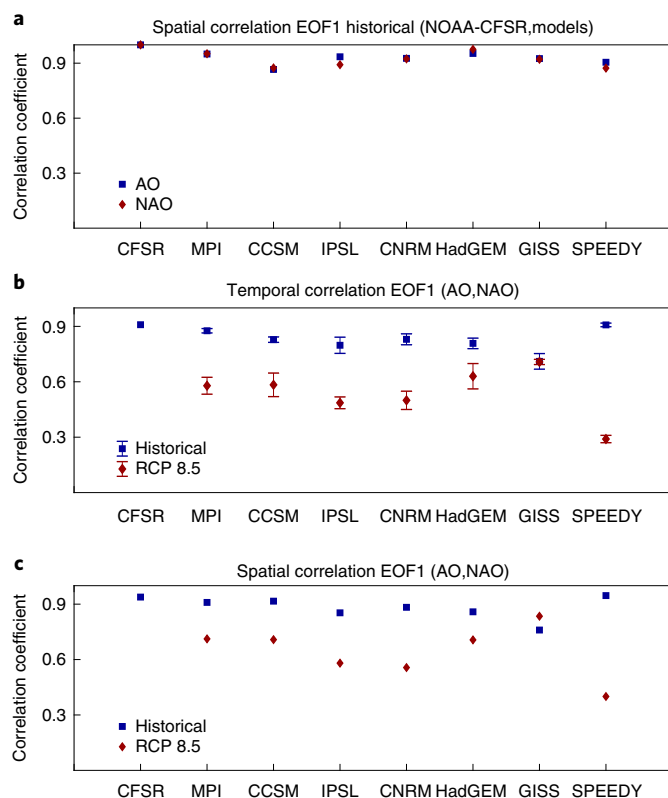


Fig. 2 | Spatial and temporal correlations. **a**, Spatial correlation coefficient of the AO and NAO reanalysis versus models in the historical simulations. **b**, Temporal correlation of monthly mean SLP (DJF) PC index, AO versus NAO (error bars indicate the standard deviation of the correlation when subsampling a 40-yr time series within the 100-yr period of historical simulations or RCP8.5 scenario). **c**, Spatial correlation of AO versus NAO in the historical simulations and RCP8.5 scenario. SLP of the hemisphere north of 20°N is regressed onto the NAO PC index and then correlated with AO. Note that SPEEDY red points refer to experiment (Pac_P) where the model is forced by warm SST in the North Pacific. All correlation coefficients are significant ($P < 0.05$).

2201 to 2300, which represents the warmest global conditions in the simulation. AO variability in a warmer climate weakens substantially over the Atlantic, while it strengthens over the Pacific (compare Fig. 1d,e to 1f). Comparison of Fig. 1g–i illustrates that no notable changes occur to the NAO pattern.

The different response of AO and NAO to a warmer climate is remarkable, considering their strong correlation in the present climate. In fact, from NOAA-CFSR reanalysis data the spatial correlation coefficient between AO and NAO patterns is 0.93 and the temporal correlation between their principal component (PC) monthly time series is 0.91. Most of the analysed models show high AO/NAO correlations in the historical period (values > 0.81 are found for all the models except for GISS), while in the warmer climate the temporal and spatial correlations mostly decrease (Fig. 2b,c). The only model that does not show a decrease in the correlations is GISS, which, as mentioned before, does not simulate a good AO pattern and has the lowest AO/NAO correlations in the historical period. Therefore it is not considered as a reliable model in this respect.

The decoupling between AO and NAO is expressed as a weakening or a disappearance of the Atlantic centre of action in the AO pattern (see Extended Data Fig. 1), while the Pacific centre of action

strengthens. The statistical insight offered by the EOF analysis can be put into perspective by focusing on the following physical mechanism. The alternating change in SLP between middle and high latitudes associated with the AO translates to latitudinal displacement of atmospheric mass, possibly due to planetary wave breaking²⁹. A negative AO phase is associated with anomalous high pressure in high latitudes and a low-pressure anomaly in mid-latitudes. The implied anomalous mass redistribution is typically expressed in the Atlantic and/or Pacific basins, not necessarily at the same time (as indicated by the lack of correlation between Pacific and Atlantic anomalies⁹).

The high correlation between NAO and AO in the current climate indicates that the preferred sector for the occurrence of the anomalous meridional eddy fluxes is the North Atlantic, which is warmer than the North Pacific during winter months and has a more variable jet stream. In the warm climate RCP8.5 scenario, the preferred sector becomes the North Pacific. We note that this change is associated with a substantially larger increase of sea surface temperature (SST) over the North Pacific compared with the North Atlantic due to the slowdown of the Atlantic Meridional Overturning Circulation^{30–32} that results in the so-called Atlantic warming hole (refs. ^{33,34} and Extended Data Fig. 2).

Moreover, in the historical period, the Icelandic low is deeper and as variable as the Aleutian low (Figs. 1a,b and 4a). In the RCP8.5 climate, the variability shifts completely to the Aleutian low, whose winter mean low pressure becomes similar to that of the Icelandic low (Figs. 1c and 4a).

In the twenty-third century RCP8.5 scenario simulations, the climate mean state differs in many aspects from the current state. To disentangle the responsible climate modification for the observed decoupling and to propose a possible explanation, we perform a simple experiment using the International Center for Theoretical Physics (ICTP) Atmospheric General Circulation Model^{35,36} ‘SPEEDY AGCM’ (Methods). We compare a control simulation (CTL), corresponding to the historical case, to a perturbation run (Pac_P), forcing the model by a 6°C Gaussian-shaped warm SST anomaly in the North Pacific ocean (experiment set up in Extended Data Fig. 3).

The two simulations are identical in their set up, except for SST boundary conditions, which simulate the differential warming of the Atlantic and the Pacific basins. Figure 4b shows that the differential warming of SPEEDY modifies the Pacific and the Atlantic low-pressure centres. The Aleutian low becomes as deep as the Icelandic low and the SLP variability in the North Pacific sector increases, as in CMIP5 RCP8.5 simulations. Results from this experiment are shown in (Figs. 2 and 4b and Extended Data Fig. 1) and show the same spatial and temporal decoupling of the AO and NAO as observed in RCP8.5 models.

The stratospheric polar vortex

In this section, stratosphere–troposphere coupling is examined in light of AO–NAO decoupling. Studies have shown that stratospheric polar vortex anomalies often force AO and NAO variability in the historical (present-day) period, through a downward propagation of the signal in the high-latitude troposphere^{11,13}. Following a similar analysis, we calculate the first EOF of November to April monthly GPH anomalies over the hemisphere north of 20°N at each pressure level independently and compute the corresponding daily NAM index (GPH PC index) time series by regressing daily GPH anomalies onto the EOF patterns (Methods). The onset of a weak polar vortex (WPV) event (identified as day0) is defined when the non-dimensional NAM index at 10 hPa is less than or equal to -1.5 .

Figure 3 shows a composite of the time–height development of the NAM index 3 months before and after the onset of WPV events, for (Fig. 3a) NOAA-CFSR reanalysis, and the MPI-ESM-LR model for (Fig. 3b) historical simulations and (Fig. 3c) RCP8.5 simulations.

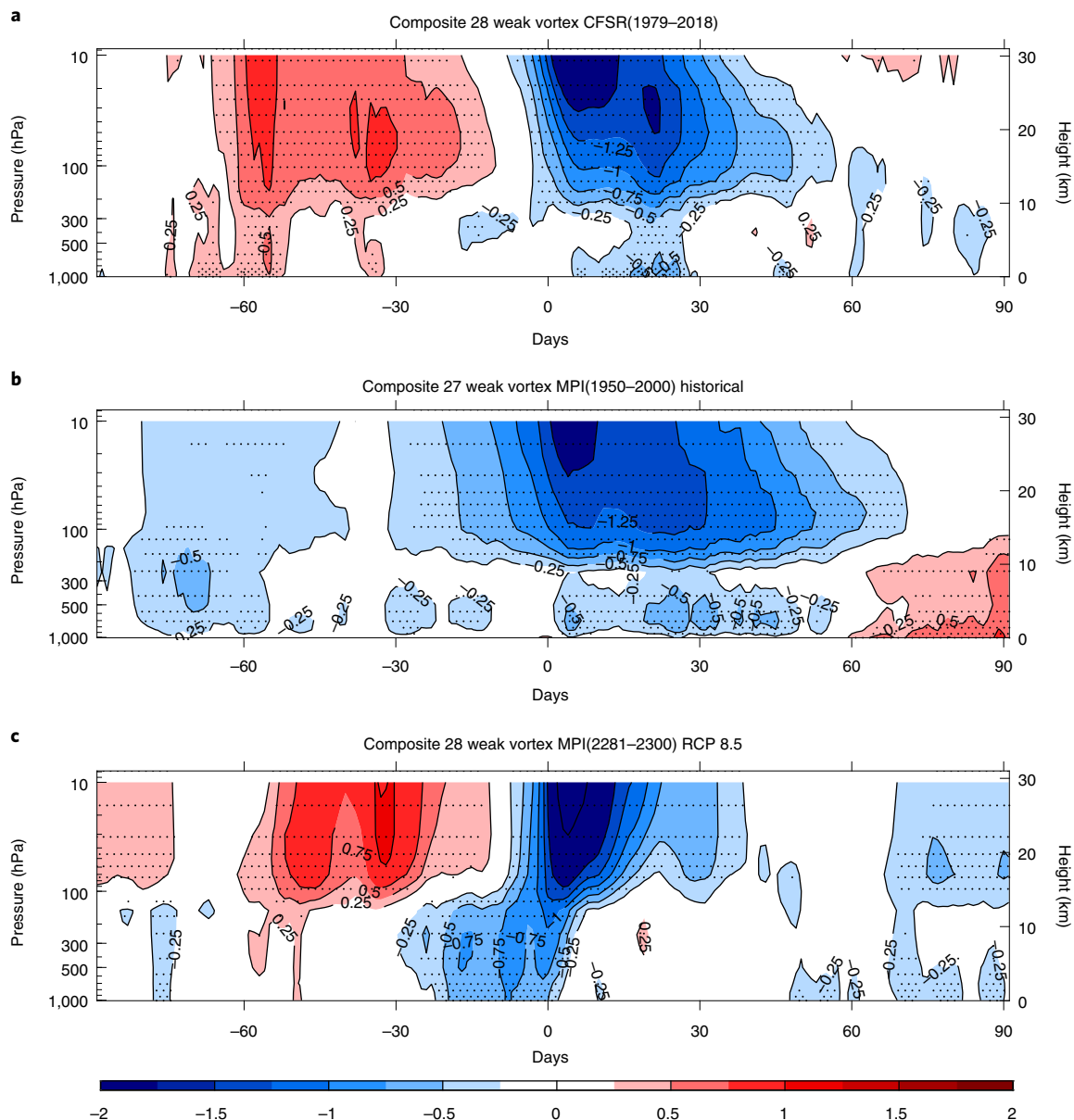


Fig. 3 | Stratosphere–troposphere coupling: weak polar vortex. a–c, Composite of time–height development of WPV events using NAM index (dimensionless) for NOAA-CFSR reanalysis (**a**), MPI historical simulations (**b**) and MPI RCP 8.5 simulations (**c**). The condition for a WPV event is when the 10 hPa NAM index is less than or equal to -1.5 . Stippling shows the 95% statistically significant anomalies using bootstrapping approach.

Composites of strong polar vortex are shown in Extended Data Fig. 4. In addition, corresponding analysis of events in the IPSL model are shown in Extended Data Fig. 5 and for SPEEDY in Extended Data Fig. 6.

Reanalysis and model historical results both show that, on average, in the present climate, the WPV signal propagates downward from the stratosphere triggering a negative AO phase on the surface within 2–4 weeks (consistent with ref. ¹¹). This top-down forcing generates high-pressure anomalies over the Arctic and the associated low-pressure anomalies over the Pacific and Atlantic mid-latitudes. Both AO and NAO are triggered by the same stratospheric conditions.

Remarkably, in RCP 8.5, surface signals precede the onset of a WPV event. It has already been shown that surface conditions, such as sea-ice or snow cover anomalies, can excite Rossby waves that propagate into the stratosphere affecting the polar vortex^{20–22,24,25}.

Here, surface anomalies preceding the onset of WPV events in MPI RCP 8.5 scenario and SPEEDY Pac_P experiment are shown in Fig. 4c,d (also Extended Data Fig. 9, where the same plot is reproduced for IPSL model) as the composite of GPH anomalies for the average of 15–10 d before a WPV event. A strong low pressure over the Pacific and a high pressure over Eurasia lead the stratospheric anomaly. This pattern projects onto the negative AO conditions in the Pacific sector (strong anomalies of opposite signs over the Arctic and over the mid-latitudes in the Pacific, where SLP has a pronounced negative anomaly).

From these results, it can be inferred that in the current climate, the stratospheric polar vortex influences the occurrence of AO events (Fig. 3a,b), while in a warmer climate that is not the case (Fig. 3c); if anything, information flows in the opposite direction and the surface AO could be used to predict the state of the stratospheric vortex.

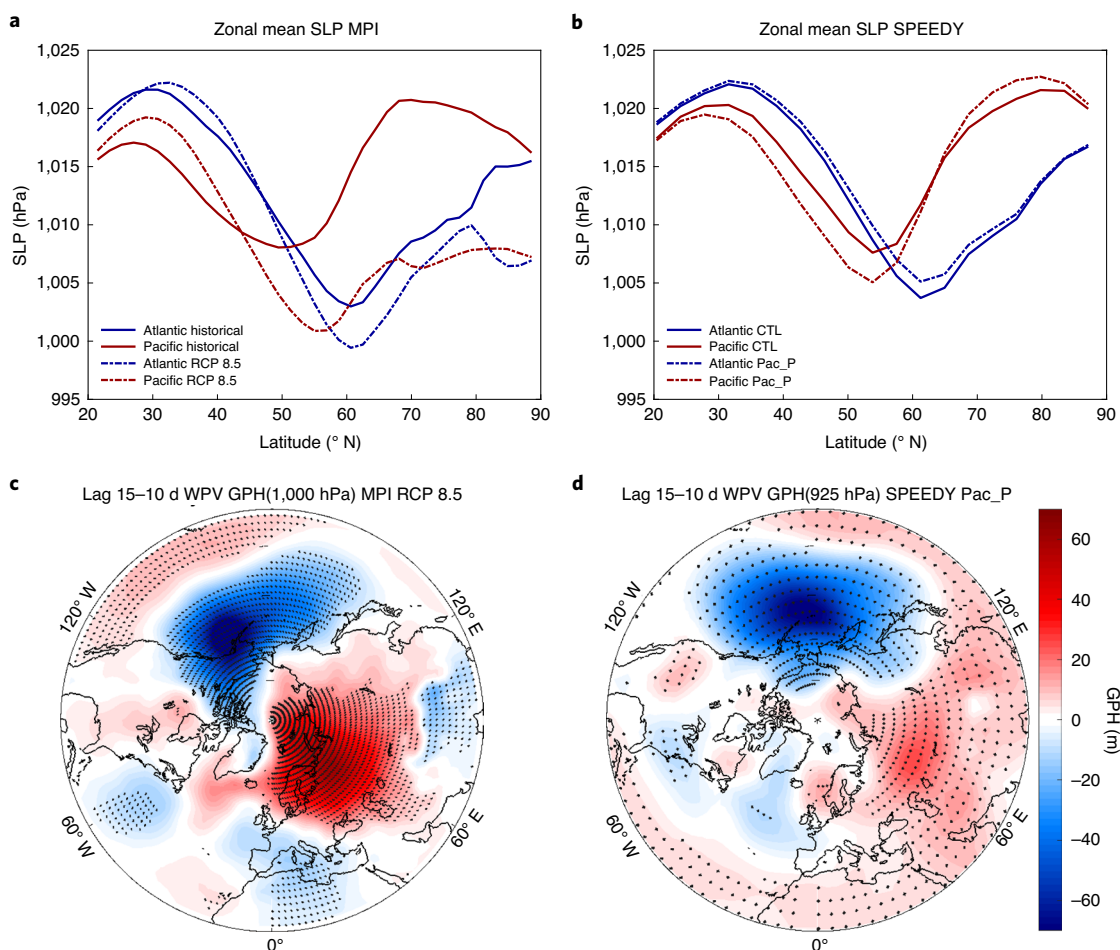


Fig. 4 | Climatology response and natural variability. a, b, Zonal mean SLP climatology for the Atlantic and the Pacific sectors for MPI (**a**) and SPEEDY (**b**). Unit: hPa. The Atlantic sector is between 80° W and 0° E (blue lines). The Pacific sector is between 130° E and 130° W (red lines). **c, d**, GPH composites of 15–10 d before the onset of weak polar vortex events for 1,000 hPa MPI RCP 8.5 scenario (**c**), 925 hPa SPEEDY Pac_P experiment (**d**) (corresponds to the upward propagating surface anomalies in Fig. 3c and Extended Data Fig. 6b). Regions of 95% statistically significant anomalies are stippled, on the basis of a standard two-sided Student's *t*-test.

The high correlation between AO and NAO in the current climate implies that the polar vortex influences both the AO and the NAO equally. We follow a similar analysis to investigate explicitly how the polar vortex influences the NAO. GPH PC time series are calculated independently for each pressure level, except that in this case they are calculated for the NAO domain.

The result shows that, in the reanalysis and in the historical simulations, the weak polar vortex propagates downward to the surface, where a negative NAO appears (ref. ³⁷ and Extended Data Figs. 7a,b and 8a,b). Similarly, in RCP 8.5, a downward propagation of the signal in the stratosphere is present and the surface NAO signal coincides with the weak polar vortex onset (Extended Data Figs. 7c and 8b). Some weak anomalies are observed in IPSL for the Atlantic sector before the onset of the WPV, due to the extension of the Eurasian high-pressure anomalies to the Atlantic as in Extended Data Fig. 9. Thus, there is no indication of the tropospheric signal in the Atlantic preceding that of the stratosphere in the warm climate, as found for the Pacific sector.

The main limitation of the analysis is that it has been performed on two models only, being the only CMIP5 models for which daily data are available for the RCP8.5 extended runs. These models (MPI-ESM-LR and IPSL-CM5A-LR), however, have a good representation of stratospheric variability³⁸, while many other CMIP5

models are known to capture weakly the downward propagation of stratospheric anomalies into the troposphere³⁹, possibly due to their low vertical resolution near and above the tropopause⁴⁰. Another caution that must be considered is that CMIP5 models are known to have biases in the representation of variability modes in the historical period⁴¹, particularly when computing winter seasonal (DJF means) AO variability. However, MPI-ESM-LR model performs exceptionally well in comparison to reanalysis in this regard and has thus been used here as a preferred model.

Conclusion

The breakdown of the connection between the AO and the NAO in the warm climate projections shows that not only the mean atmospheric circulation changes but also the modes of variability of the mid- to high-latitude atmosphere are dramatically modified. The leading hemispheric-EOF (AO) changes substantially in a warmer climate, while the leading regional (Atlantic) EOF (NAO) is more stable. The results support the fact that these patterns of variability, which are defined to maximize variance, are not some fundamental vibrational mode of the climate system but patterns that can change in response to changes in the climate. The AO–NAO break up is associated with a different connection to the stratospheric variability, which is now recognized as a precursor of the tropospheric

signals, while it appears to be triggered by the Pacific and Eurasian surface anomalies in the warm climate.

Online content

Any methods, additional references, Nature Research reporting summaries, source data, extended data, supplementary information, acknowledgements, peer review information; details of author contributions and competing interests; and statements of data and code availability are available at <https://doi.org/10.1038/s41558-020-00966-8>.

Received: 26 December 2019; Accepted: 12 November 2020;
Published online: 11 January 2021

References

- Walker, G. T. & Bliss, E. W. World weather V. *Mem. R. Meteorol. Soc.* **4**, 53–84 (1932).
- Hurrell, J. W. Decadal trends in the North Atlantic Oscillation: regional temperatures and precipitation. *Science* **269**, 676–679 (1995).
- Thompson, D. W. J. & Wallace, J. M. The Arctic Oscillation signature in the wintertime geopotential height and temperature fields. *Geophys. Res. Lett.* **25**, 1297–1300 (1998).
- Thompson, D. & Wallace, J. Annular modes in the extratropical circulation. Part I: Month-to-month variability. *J. Clim.* **13**, 1000–1016 (2000).
- Thompson, D. W. J., Wallace, J. M. & Hegerl, G. C. Annular modes in the extratropical circulation. Part II: Trends. *J. Clim.* **13**, 1018–1036 (2000).
- Cohen, J. et al. Recent Arctic amplification and extreme mid-latitude weather. *Nat. Geosci.* **7**, 627–637 (2014).
- Ambaum, M. H. P., Hoskins, B. J. & Stephenson, D. B. Arctic Oscillation or North Atlantic Oscillation? *J. Clim.* **14**, 3495–3507 (2001).
- Wanner, H. et al. North Atlantic Oscillation—concepts and studies. *Surv. Geophys.* **22**, 321–381 (2001).
- Deser, C. On the teleconnectivity of the ‘Arctic Oscillation’. *Geophys. Res. Lett.* **27**, 779–782 (2000).
- Holland, M. M. The North Atlantic Oscillation–Arctic Oscillation in the CCSM2 and its influence on Arctic climate variability. *J. Clim.* **16**, 2767–2781 (2003).
- Baldwin, M. P. & Dunkerton, T. J. Stratospheric harbingers of anomalous weather regimes. *Science* **294**, 581–584 (2001).
- Cohen, J. & Barlow, M. The NAO, the AO, and global warming: how closely related? *J. Clim.* **18**, 4498–4513 (2005).
- Baldwin, M. & Dunkerton, T. Propagation of the Arctic Oscillation from the stratosphere to the troposphere. *J. Geophys. Res.* **104**, 30937–30946 (1999).
- Butler, A. H. & Polvani, L. M. El Niño, La Niña, and stratospheric sudden warmings: a reevaluation in light of the observational record. *Geophys. Res. Lett.* <https://doi.org/10.1029/2011GL048084> (2011).
- Baldwin, M. P. et al. The quasi-biennial oscillation. *Rev. Geophys.* **39**, 179–229 (2001).
- Jiang, Z., Feldstein, S. B. & Lee, S. The relationship between the Madden–Julian Oscillation and the North Atlantic Oscillation. *Q. J. R. Meteorol. Soc.* **143**, 240–250 (2017).
- Garfinkel, C. I., Feldstein, S. B., Waugh, D. W., Yoo, C. & Lee, S. Observed connection between stratospheric sudden warmings and the Madden–Julian Oscillation. *Geophys. Res. Lett.* **39**, L18807 (2012).
- Kang, W. & Tziperman, E. More frequent sudden stratospheric warming events due to enhanced MJO forcing expected in a warmer climate. *J. Clim.* **30**, 8727–8743 (2017).
- Wu, Q. & Zhang, X. Observed forcing-feedback processes between northern hemisphere atmospheric circulation and arctic sea ice coverage. *J. Geophys. Res.* <https://doi.org/10.1029/2009JD013574> (2010).
- Peings, Y. & Magnusdottir, G. Response of the wintertime Northern Hemisphere atmospheric circulation to current and projected Arctic sea ice decline: a numerical study with CAM5. *J. Clim.* **27**, 244–264 (2014).
- García-Serrano, J., Frankignoul, C., Gastineau, G. & de la Cámara, A. On the predictability of the winter Euro-Atlantic climate: lagged influence of autumn Arctic sea ice. *J. Clim.* **28**, 5195–5216 (2015).
- Ruggieri, P., Kucharski, F., Buizza, R. & Ambaum, M. H. P. The transient atmospheric response to a reduction of sea-ice cover in the Barents and Kara Seas. *Q. J. R. Meteorol. Soc.* **143**, 1632–1640 (2017).
- Kretschmer, M., Coumou, D., Donges, J. F. & Runge, J. Using causal effect networks to analyze different arctic drivers of midlatitude winter circulation. *J. Clim.* **29**, 4069–4081 (2016).
- Nakamura, T. et al. The stratospheric pathway for Arctic impacts on midlatitude climate. *Geophys. Res. Lett.* **43**, 3494–3501 (2016).
- Cohen, J., Barlow, M., Kushner, P. & Saito, K. Stratosphere–troposphere coupling and links with Eurasian land surface variability. *J. Clim.* **20**, 5335–5343 (2007).
- Deser, C., Tomas, R. A. & Peng, S. The transient atmospheric circulation response to North Atlantic SST and sea ice anomalies. *J. Clim.* **20**, 4751–4767 (2007).
- Hurrell, J. W. & Deser, C. North Atlantic climate variability: the role of the North Atlantic Oscillation. *J. Marine Syst.* **78**, 28–41 (2009).
- Saha, S. et al. The NCEP climate forecast system reanalysis. *Bull. Am. Meteorol. Soc.* **91**, 1015–1058 (2010).
- Polvani, L. M. & Saravanan, R. The three-dimensional structure of breaking Rossby waves in the polar wintertime stratosphere. *J. Atmos. Sci.* **57**, 3663–3685 (2000).
- Chen, C., Wang, G., Xie, S.-P. & Liu, W. Why does global warming weaken the Gulf Stream but intensify the Kuroshio? *J. Clim.* **32**, 7437–7451 (2019).
- Sévellec, F., Fedorov, A. & Liu, W. Arctic sea-ice decline weakens the Atlantic Meridional Overturning Circulation. *Nat. Clim. Change* **7**, 604–610 (2017).
- Rahmstorf, S. et al. Exceptional twentieth-century slowdown in Atlantic Ocean overturning circulation. *Nat. Clim. Change* **5**, 475–480 (2015).
- Hartman, D. et al. in *Climate Change 2013: The Physical Science Basis* (eds Stocker, T. F. et al.) 159–254 (Cambridge Univ. Press, 2013).
- Alexander, M. et al. Projected sea surface temperatures over the 21st century: changes in the mean, variability and extremes for large marine ecosystem regions of northern oceans. *Elem. Sci. Anthropol.* **6**, 9 (2018).
- Molteni, F. Atmospheric simulations using a GCM with simplified physical parameterizations. I: Model climatology and variability in multi-decadal experiments. *Clim. Dynam.* **20**, 175–191 (2003).
- Kucharski, F. et al. On the need of intermediate complexity General Circulation Models: a ‘SPEEDY’ example. *Bull. Am. Meteorol. Soc.* **94**, 25–30 (2013).
- Ayarzagüena, B. et al. Uncertainty in the response of sudden stratospheric warmings and stratosphere–troposphere coupling to quadrupled CO₂ concentrations in CMIP6 models. *J. Geophys. Res.* **125**, e2019JD032345 (2020).
- Charlton-Perez, A. J. et al. On the lack of stratospheric dynamical variability in low-top versions of the CMIP5 models. *J. Geophys. Res.* **118**, 2494–2505 (2013).
- Furtado, J. C., Cohen, J. L., Butler, A. H., Riddle, E. E. & Kumar, A. Eurasian snow cover variability and links to winter climate in the CMIP5 models. *Clim. Dynam.* **45**, 2591–2605 (2015).
- Richter, J. H., Solomon, A. & Bacmeister, J. T. Effects of vertical resolution and nonorographic gravity wave drag on the simulated climate in the Community Atmosphere Model, Version 5. *J. Adv. Model. Earth Syst.* **6**, 357–383 (2014).
- Gong, H., Wang, L., Chen, W., Chen, X. & Nath, D. Biases of the wintertime Arctic oscillation in CMIP5 models. *Environ. Res. Lett.* **12**, 014001 (2017).

Publisher’s note Springer Nature remains neutral with regard to jurisdictional claims in published maps and institutional affiliations.

© The Author(s), under exclusive licence to Springer Nature Limited 2021

Methods

Data. The adopted reanalysis presented in the study is obtained from the NCEP Climate Forecast System Reanalysis (CFRS)²⁸ for SLP and GPH from 1,000 to 10 hPa levels in the period from 1979 to 2018. The spatial resolution is $0.5^\circ \times 0.5^\circ$. In the Extended Data, we also present the reanalysis from the European Centre for Medium-Range Weather Forecasts (ECMWF) ERA-Interim for SLP in the period 1979 to 2018. The spatial resolution is 80 km (T255 spectral).

Model data were obtained from the CMIP5. The following CMIP5 models were used: MPI-ESM-LR^{42,43}, IPSL-CM5A-LR⁴⁴, CCSM4⁴⁵, CNRM-CM5⁴⁶, HadGEM2-ES⁴⁷ and GISS-E2-R⁴⁸. They comprise all models available for the twenty-third century in the RCP 8.5 scenario. No a-priori model selection has been performed. All models were regridded to a common $2.5^\circ \times 2.5^\circ$ resolution. The historical period includes the data from 1901 to 2000 and the considered period for (RCP 8.5) projections is from 2201 to 2300.

Definition of AO and NAO. The AO is defined³ as the leading mode of the EOF analysis for SLP anomalies for the hemisphere north of 20°N . Similarly, the NAO is defined²⁷ by calculating the leading mode of the EOF for SLP anomalies, for the domain (20°N – 80°N , 90°W – 40°E).

Monthly data for DJF are considered after removal of the climatological seasonal cycle. The data are detrended and are weighted by the square root of cosine of latitude⁴⁹ before computing the covariance matrix.

For the temporal correlation in Fig. 2b, to take into account the non-stationarity of the correlation within the 100 years of historical and RCP 8.5 simulations, the spread is obtained by randomly subsampling model runs to 40 yr (which is equivalent to the length of reanalysis), then calculating mean correlation coefficient (point) and the standard deviation (error bar), as presented in Fig. 2b.

The spatial correlation in Fig. 2a,c is calculated by regridding reanalysis and models to a common $2.5^\circ \times 2.5^\circ$ grid. In case of AO/NAO correlations, SLP anomalies north of 20°N are regressed onto the NAO index and the obtained pattern is correlated to AO pattern.

Polar vortex. For this part of the analysis, we consider the daily data of GPH from 1,000 hPa to 10 hPa for the months from November to April. For reanalysis, the period from 1979 to 2018 is used. Due to the limited availability of CMIP5 daily data in the extended RCP 8.5 simulations, the analysis is performed using two models: MPI-ESM-LR from 1950 to 2000 for the historical period and from 2281 to 2300 (and 2181–2200, not shown) for the RCP 8.5 simulation; and IPSL-CM5A-LR historical simulations from 1901 to 2000 and RCP 8.5 simulations from 2201 to 2300. Twenty-third century daily data from other models are no longer publicly available.

The calculation of the daily NAM index in each pressure level is obtained similarly⁴¹ as follows: GPH data are detrended and the climatological seasonal cycle is removed. Then data are weighted by the square root of cosine latitude. For the hemisphere north of 20°N , we calculate the first EOF of monthly NDJFMA GPH anomalies, for each pressure level from 1,000 hPa to 10 hPa independently. Then daily GPH anomalies of NDJFMA are regressed onto the EOF of each level. This results in NAM index (GPH PC index) for each pressure level.

The onset of a weak polar vortex event is defined by the 10 hPa level NAM index. When the 10 hPa index is less than or equal to -1.5 , the composite is captured for all pressure levels from -90 to $+90$ lag-lead days from the onset which is at 0 d. The same is done for strong polar vortex, except that the NAM index is ≥ 1 .

The NAM is also examined explicitly in the North Atlantic sector, by repeating the same analysis mentioned before, except that for the domain (20°N – 80°N , 90°W – 40°E) as in Extended Data Figs. 7 and 8. However, the onset of a weak polar vortex is still using the NAM index of the hemisphere north of 20°N .

Statistical significance of the results shown in Fig. 3 and similar, is done by calculating uncertainty bounds on the basis of random sampling using a bootstrapping approach. This is done by randomly sampling the same number of winters from the distribution and comparing the observed signal to the 95th percentile of the random sampling distribution.

SPEEDY AGCM simulation. The ICTP AGCM is nicknamed SPEEDY for ‘Simplified Parameterization, primitive Equation Dynamics’, which is based on a spectral dynamical core⁵⁰. It is an intermediate complexity atmospheric model, with eight vertical layers and a triangular truncation of horizontal spectral fields at total wave number 30. It is a hydrostatic, σ -coordinate, spectral transform model in the vorticity-divergence form⁵¹. The parameterized processes include short- and long-wave radiation, large-scale condensation, convection, surface fluxes of momentum, heat, moisture and vertical diffusion. Convection is represented by a mass-flux scheme that is activated where conditional instability is present and boundary-layer fluxes are obtained by stability-dependent bulk formulae. Further description of the model is in refs. ^{35,36}. The representation of the NAO and some applications using the model can be found in refs. ^{52,53}. Despite the low-lid stratosphere (30 hPa), the model is able to capture troposphere–stratosphere interactions, such as the triggering of a negative NAO through the stratosphere due to reduced sea ice in Barent and Kara seas²². Note that, for the stratosphere–troposphere coupling, the onset of WPV events is based on NAM index of 30 hPa,

considering the EOF that spatially corresponds to the polar vortex and AO in all pressure levels.

We conduct two simulations; each simulation is 50 yr long from 1961 to 2010. A CTL has monthly prescribed climatological SSTs using Hadley Center (HadSST) data. A Pac_P is the same as CTL, except that in the North Pacific we add a persistent Gaussian-shaped SST warming with a peak of 6°C to qualitatively mimic the relative SST conditions in the Pacific and the Atlantic in RCP 8.5 (that is, North Pacific ocean warmer than North Atlantic ocean). Extended Data Fig. 3 shows the SST forcing used in the experiment.

Data availability

All CMIP5 data used in this study are available on Earth System Grid Federation (ESGF) on the following link: <https://esgf-node.llnl.gov/search/esgf-llnl/>. NOAA-CFSR reanalysis data are available at <https://www.ncdc.noaa.gov>. ERA-Interim reanalysis data are available at <https://www.ecmwf.int/>.

Code availability

The ICTP AGCM ‘SPEEDY model’ can be downloaded by contacting F. Kucharski (kucharsk@ictp.it) or as indicated in the following link: <https://www.ictp.it/research/esp/models/speedy.aspx>. Codes used to set up model simulations, analyse data and create figures can be provided upon request from the corresponding author.

References

- Raddatz, T. et al. Will the tropical land biosphere dominate the climate–carbon cycle feedback during the twenty-first century? *Clim. Dynam.* **29**, 565–574 (2007).
- Marstrand, S. et al. The Max-Planck-Institute global ocean/sea ice model with orthogonal curvilinear coordinates. *Ocean Model.* **5**, 91–127 (2003).
- Dufresne, J.-L., Foujols, M.-A. & Denvil, Sea Climate change projections using the IPSL-CM5 earth system model: from CMIP3 to CMIP5. *Clim. Dynam.* **40**, 2123–2165 (2013).
- Gent, P. R. et al. The Community Climate System Model Version 4. *J. Clim.* **24**, 4973–4991 (2011).
- Voldoire, A., Sanchez-Gomez, E. & Salas y Mélia, Dea The CNRM-CM5.1 global climate model description and basic evaluation. *Clim. Dynam.* **40**, 2091–2121 (2013).
- Johns, T. C. et al. The New Hadley Centre Climate Model (HadGEM1): evaluation of coupled simulations. *J. Clim.* **19**, 1327–1353 (2006).
- Schmidt, G. A. et al. Configuration and assessment of the GISS ModelE2 contributions to the CMIP5 archive. *J. Adv. Model. Earth Syst.* **6**, 141–184 (2014).
- North, G., Bell, T., Cahalan, R. & Moeng, F. Sampling errors in the estimation of empirical orthogonal functions. *Mon. Weather Rev.* **110**, 699–706 (1982).
- Held, I. M. & Suarez, M. J. A proposal for the intercomparison of the dynamical cores of atmospheric general circulation models. *Bull. Am. Meteorol. Soc.* **75**, 1825–1830 (1994).
- Bourke, W. A multi-level spectral model. i. formulation and hemispheric integrations. *Mon. Weather Rev.* **102**, 687–701 (1974).
- Kucharski, F. & Molteni, F. On non-linearities in a forced North Atlantic Oscillation. *Clim. Dynam.* **21**, 677–687 (2003).
- Kucharski, F., Molteni, F. & Bracco, A. Decadal interactions between the Western Tropical Pacific and the North Atlantic Oscillation. *Clim. Dynam.* **26**, 79–91 (2006).

Acknowledgements

We acknowledge the World Climate Research Programme’s Working Group on Coupled Modelling, which is responsible for the Coupled Model Intercomparison Project (CMIP), and thank the climate modelling groups (listed in Data availability) for producing and making available their model output. M.E.H. and C.P. gratefully acknowledge hospitality from the Department of Earth and Planetary Sciences, Harvard University, during part of this work. M.E.H. was supported by Cariplo Foundation, EXTRA project and HPC-TRES grant no. 2017-03. This article is an outcome of Progetto Dipartimenti di Eccellenza, funded by MIUR. We acknowledge CINECA HPC grant no. IsC65_CSIPAR and FAQC UniMiB grant. M.E.H. would like to thank F. Kucharski for providing SPEEDY model and for the insightful discussions. E.T. was supported by the NSF Climate Dynamics programme grant no. AGS-1924538, and thanks the Weizmann Institute of Science for its hospitality during parts of this work.

Author contributions

M.E.H. conducted the simulations and analysed the data. The three authors equally contributed to conceiving and designing the study, interpreting the results and writing the manuscript.

Competing interests

The authors declare no competing interests.

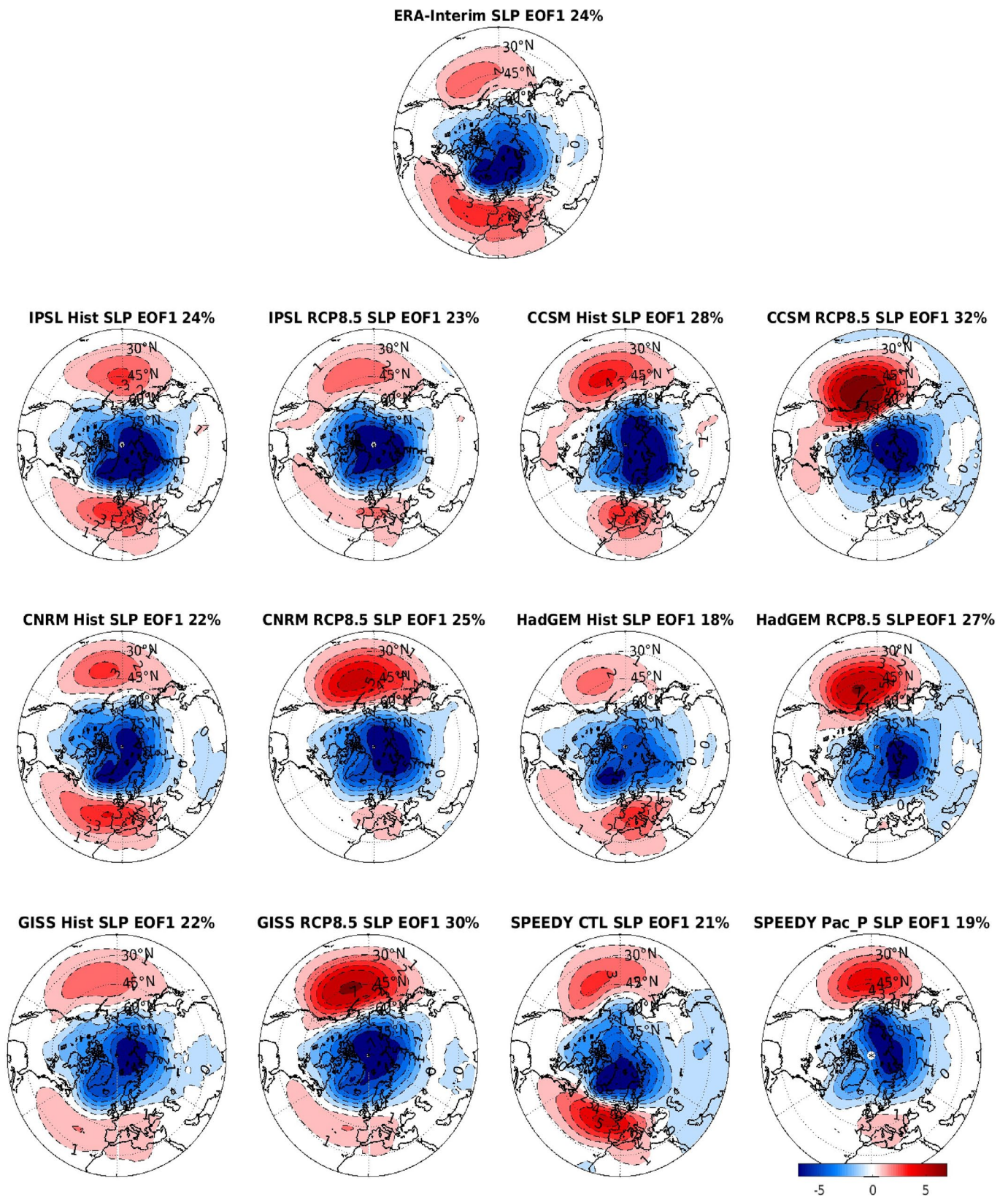
Additional information

Extended data is available for this paper at <https://doi.org/10.1038/s41558-020-00966-8>.

Correspondence and requests for materials should be addressed to M.E.H.

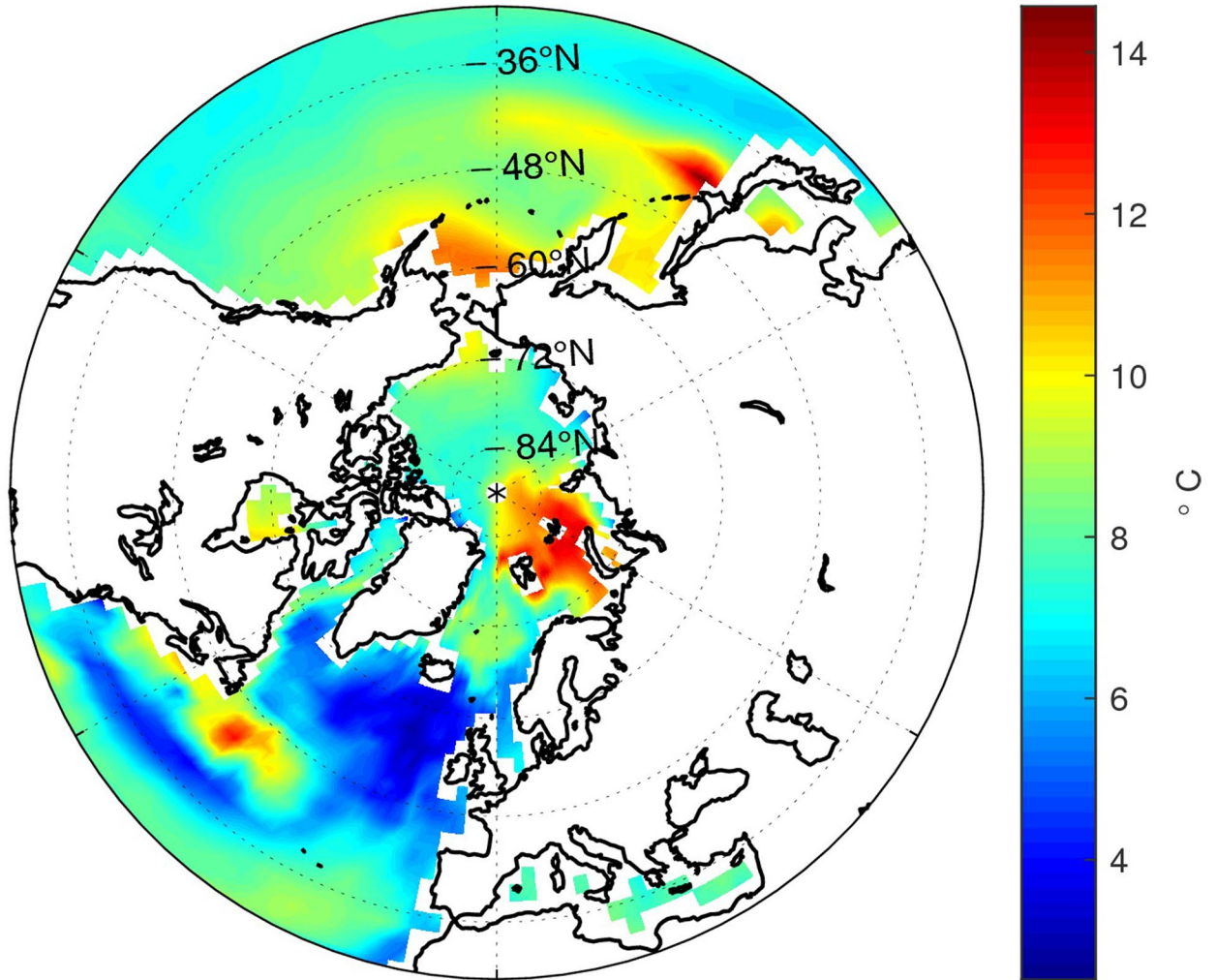
Peer review information *Nature Climate Change* thanks Edwin Gerber and the other, anonymous, reviewer(s) for their contribution to the peer review of this work.

Reprints and permissions information is available at www.nature.com/reprints.



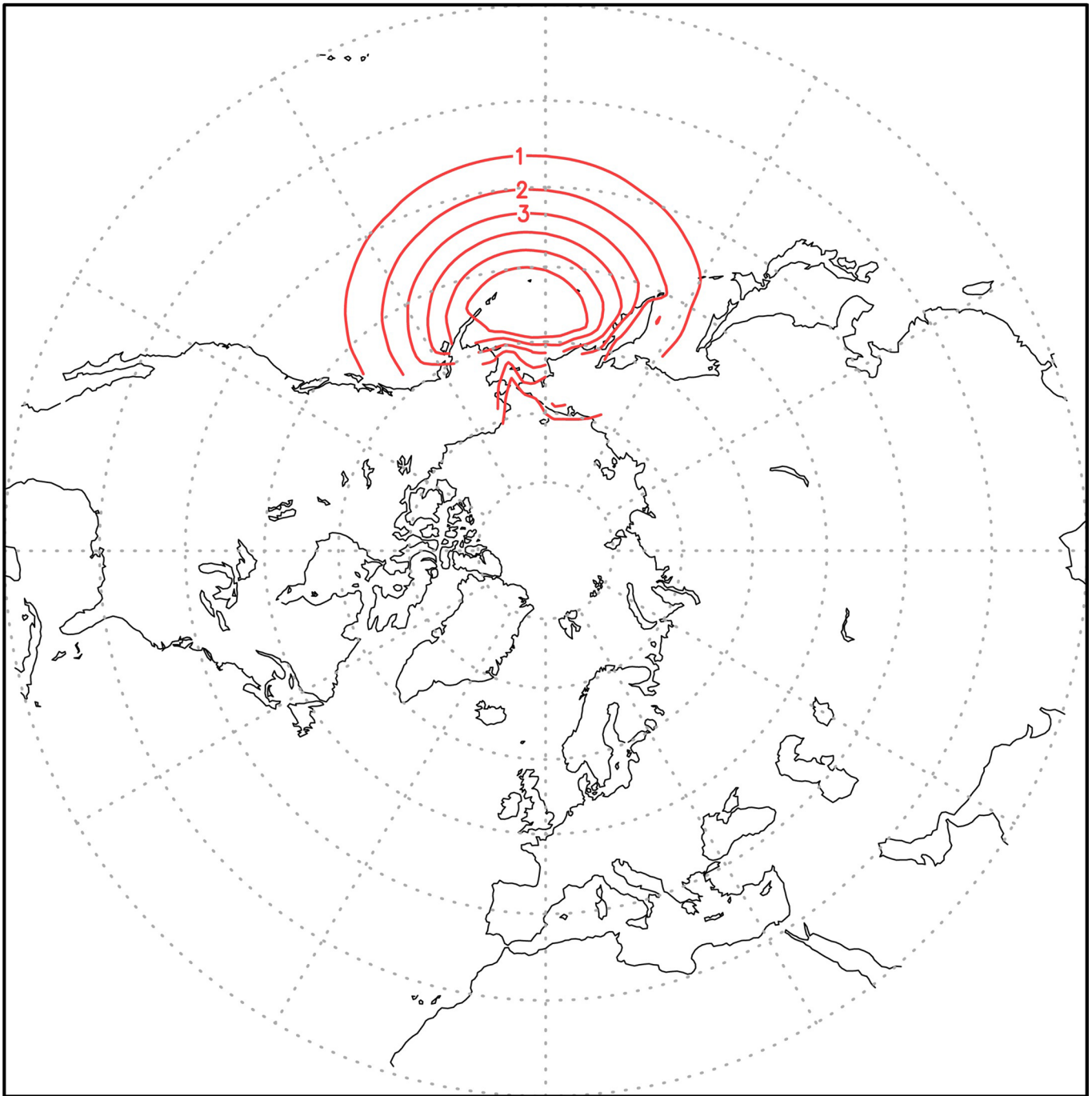
Extended Data Fig. 1 | The Arctic Oscillation in ERA-Interim reanalysis, historical and RCP8.5. The leading EOF mode (AO) for wintertime (DJF) sea-level pressure (SLP) for Historical (Hist) and RCP8.5 in CMIP5 models. Note that SPEEDY panels refer to the control run using climatology (CTL) and for Pacific SST perturbation run (Pac_P). (Unit: hPa corresponding to 1 standard deviation of the PC). Explained variance by the EOF is indicated on top.

Sea Surface Temperature DJF MPI RCP8.5-Historical

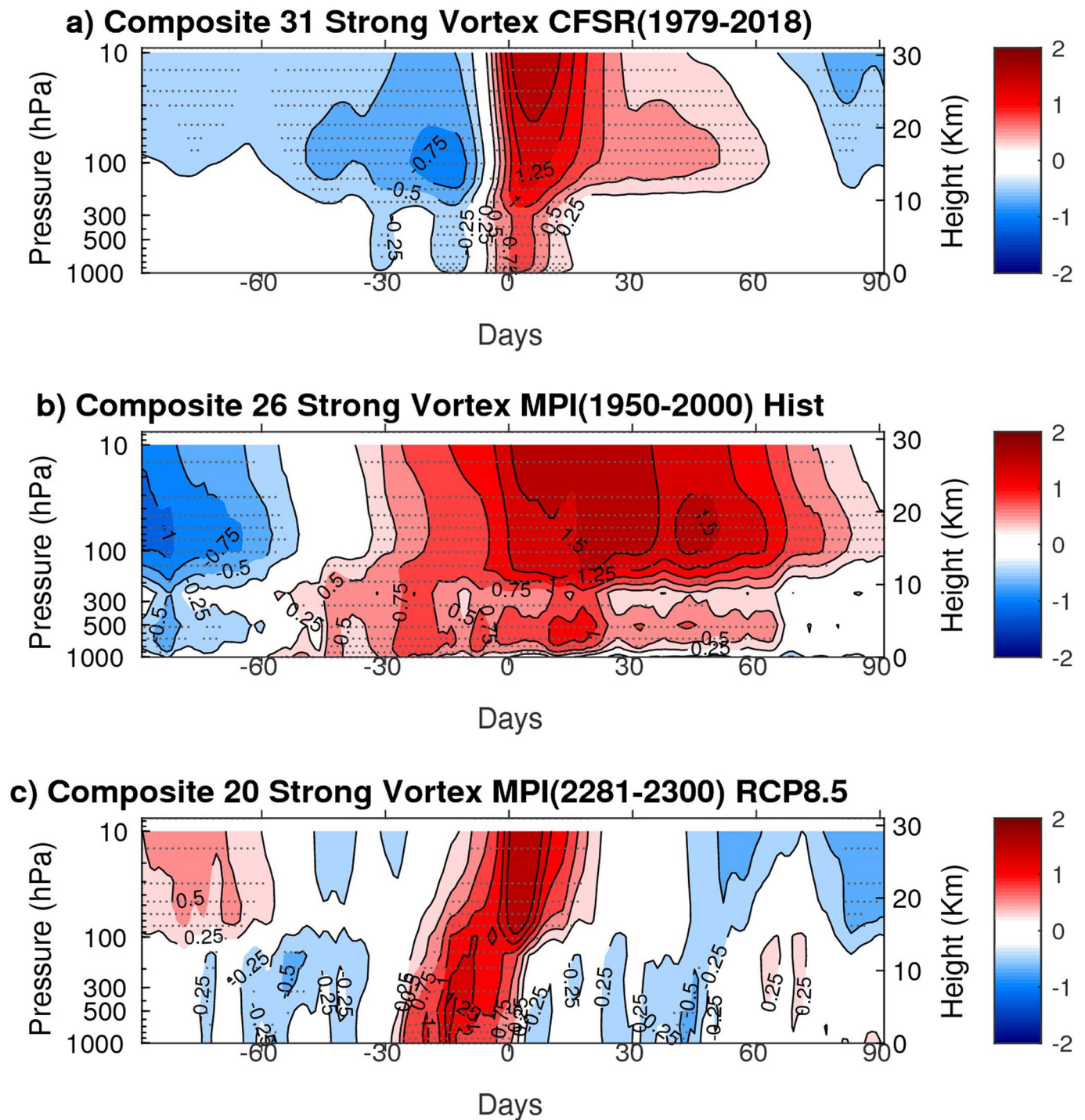


Extended Data Fig. 2 | Pacific ocean SST response is stronger than the Atlantic. Climatology response of DJF sea surface temperature (RCP8.5-Historical) from MPI-ESM-LR.

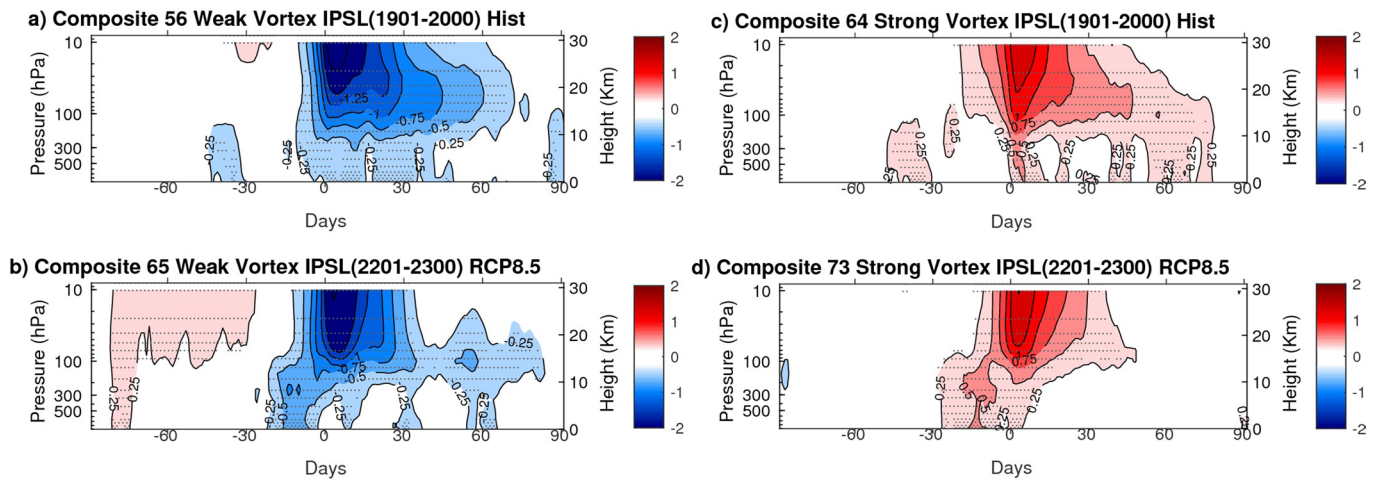
SPEEDY SST Forcing: Pac_P-CTL



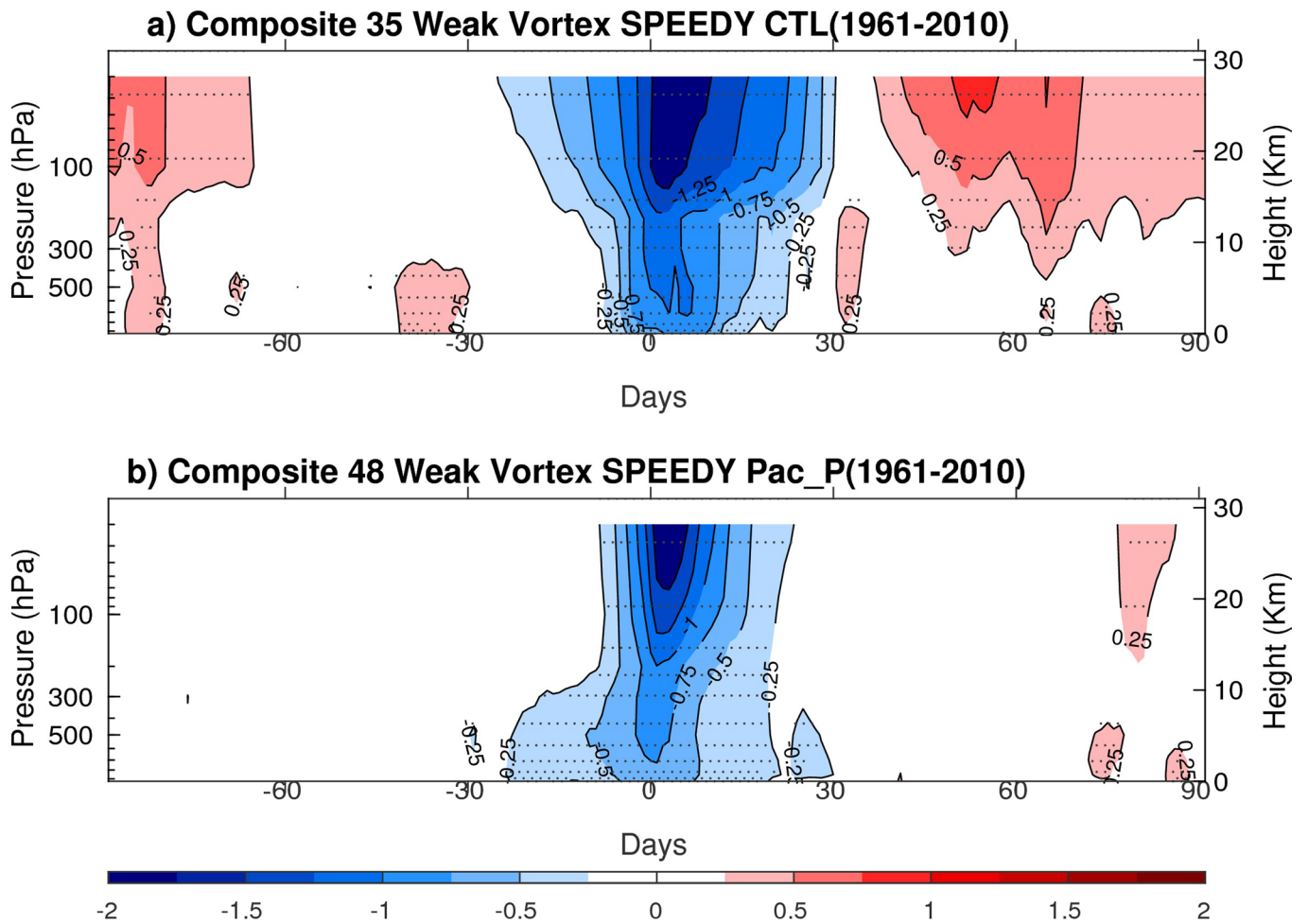
Extended Data Fig. 3 | SPEEDY General Circulation Model set up. SPEEDY SST forcing design for Pac_P run: Positive Gaussian SST in the North Pacific Ocean with a peak of 6°C.



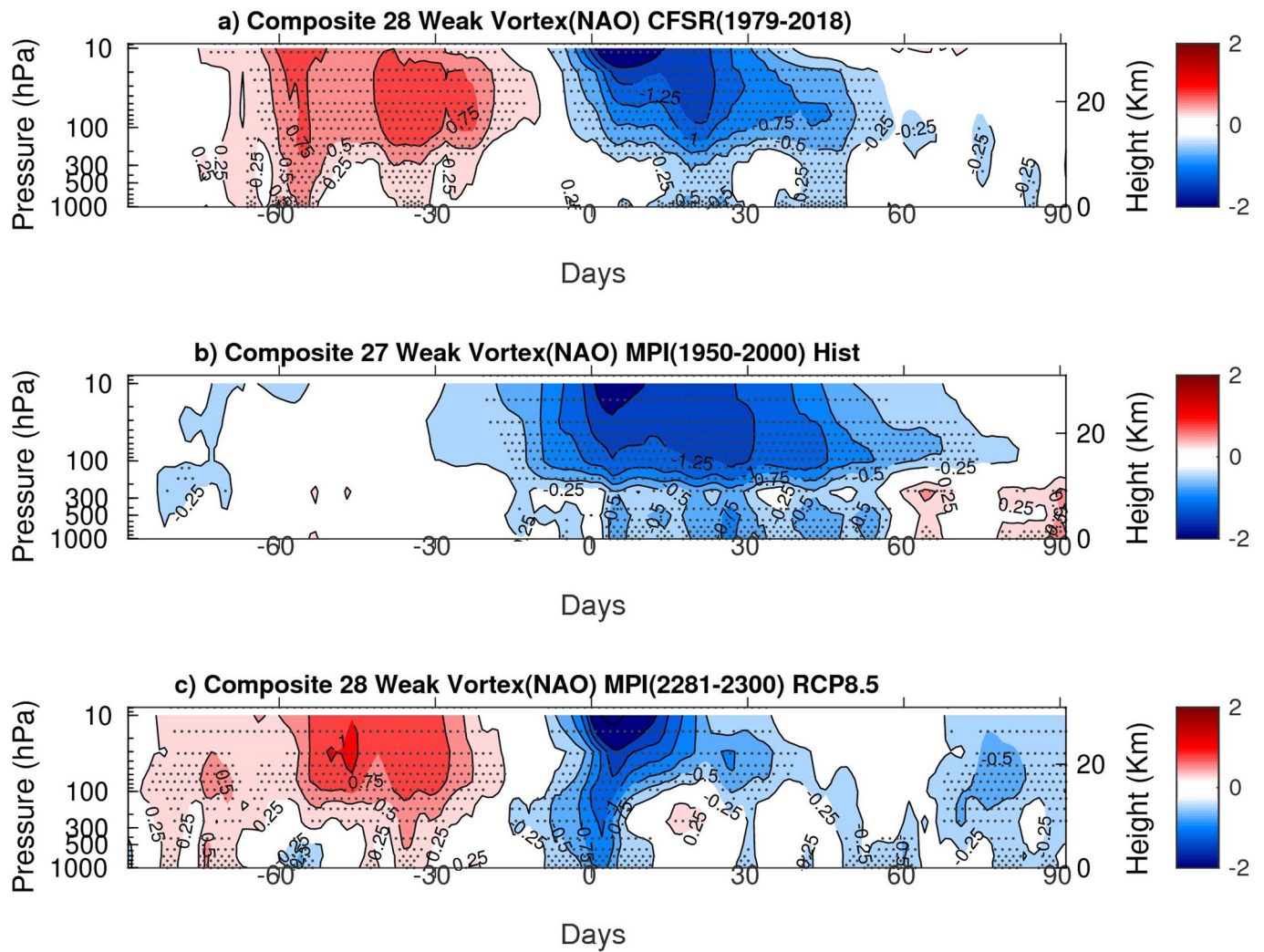
Extended Data Fig. 4 | Strong Polar Vortex. **a**, Same as fig. 3 except that it is for the strong polar vortex (SPV). The condition for a SPV event is when the 10 hPa NAM index is $\geq +1$. Stippling shows the 95% statistically significant anomalies using bootstrapping approach.



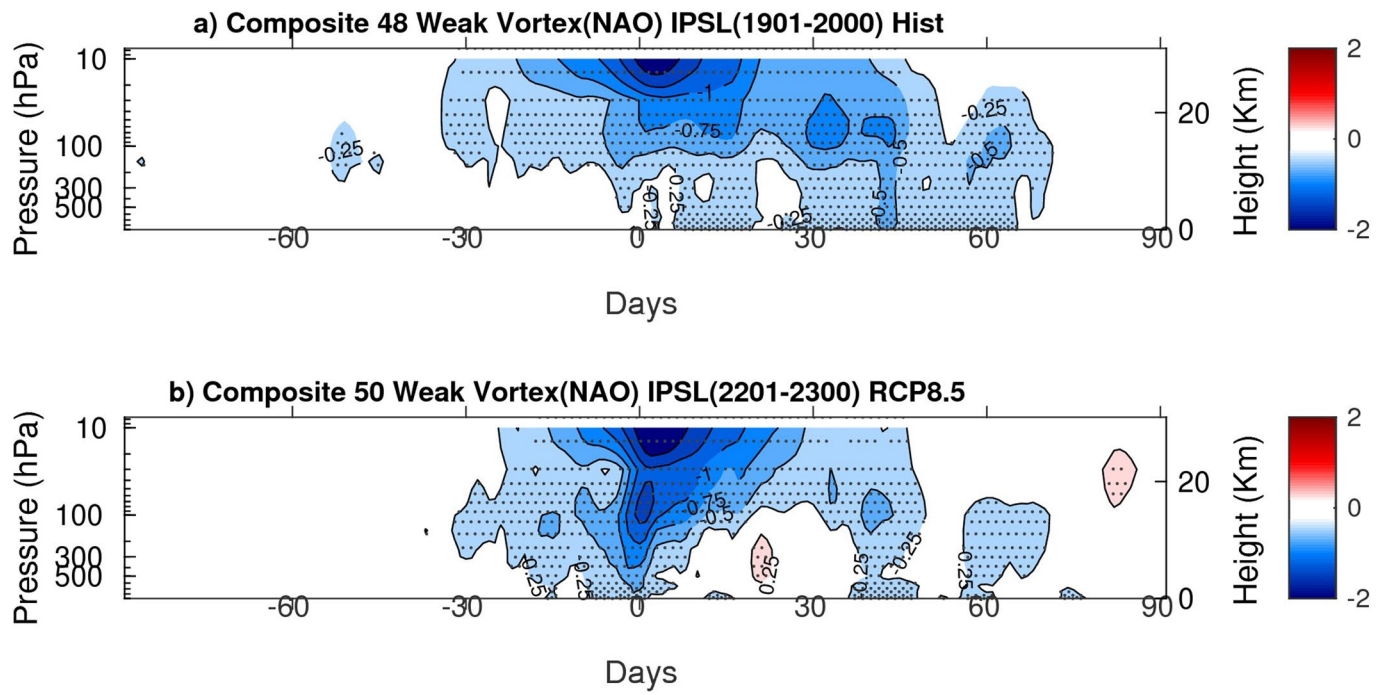
Extended Data Fig. 5 | Weak polar vortex in IPSL-CM5A-LR. a, Same as Fig. 3 & extended data Fig. 4, except that it is for IPSL-CM5A-LR.



Extended Data Fig. 6 | Weak polar vortex in SPEEDY AGCM experiment. a, Same as fig. 3, except that it is for SPEEDY AGCM. Note that the condition for the onset is based on NAM index at 30 hPa.

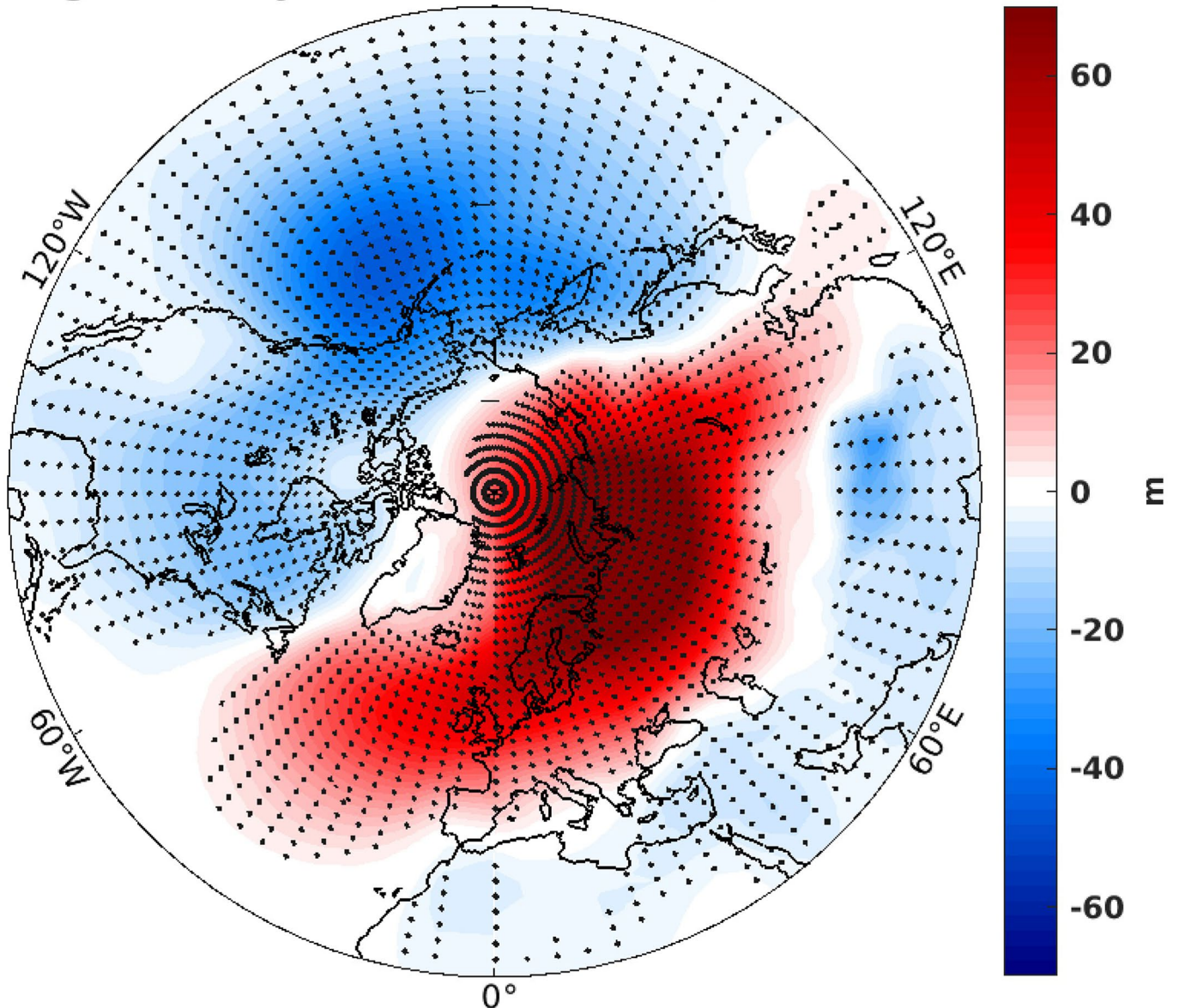


Extended Data Fig. 7 | Polar vortex influence in the Atlantic sector. Same as in fig. 3, except that here NAM index is for NAO domain instead of AO domain. The condition for the onset is still when the 10 hPa NAM index is ≤ -1.5 for weak polar vortex. **a.** CFSR reanalysis. **b.** MPI historical. **c.** MPI RCP8.5. Stippling indicates the 95% statistically significant anomalies using boot-strapping approach.



Extended Data Fig. 8 | Polar vortex influence in the Atlantic sector. Same as in extended data Fig. 7, except for IPSL-CM5A-LR model.

Lag 15-10 days WPV GPH(1000hPa) IPSL RCP8.5



Extended Data Fig. 9 | Eurasian high and Aleutian low-pressure centres leading weak polar vortex. Same as in fig. 4a, except for IPSL-CM5A-LR. (corresponds to the upward propagating surface anomalies in extended data fig. 5b).